IEEE Photonics Journal
An IEEE Photonics Society Publication

Open Access

Generation of Uncorrelated Multichannel Chaos by Electrical Heterodyning for Multiple-Input–Multiple-Output Chaos Radar Application

Volume 8, Number 1, February 2016

Chih-Hao Cheng
Yi-Cheng Chen
Fan-Yi Lin

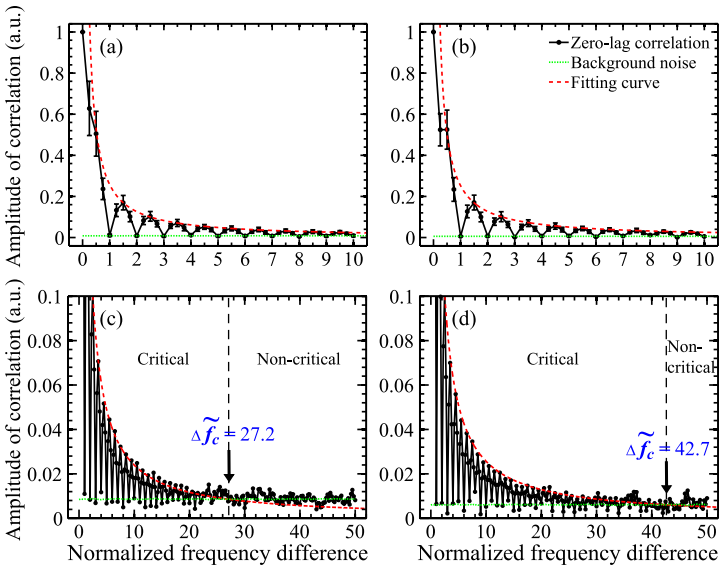

DOI: 10.1109/JPHOT.2015.2510327
1943-0655 © 2015 IEEE

Generation of Uncorrelated Multichannel Chaos by Electrical Heterodyning for Multiple-Input–Multiple-Output Chaos Radar Application

Chih-Hao Cheng, Yi-Cheng Chen, and Fan-Yi Lin

Institute of Photonics Technologies, Department of Electrical Engineering, National Tsing Hua University, Hsinchu 300, Taiwan

DOI: 10.1109/JPHOT.2015.2510327

Manuscript received November 19, 2015; revised December 15, 2015; accepted December 15, 2015. Date of publication December 22, 2015; date of current version December 29, 2015. This work was supported in part by the Ministry of Science and Technology of Taiwan under Contract MOST 103-2112-M-007-019-MY3 and in part by the National Tsing Hua University under Grant 104N2081E1. Corresponding author: F.-Y. Lin (e-mail: fylin@ee.nthu.edu.tw).

Abstract: Multiple-input–multiple-output (MIMO) radar has received much attention in recent years for its great ability in imaging. However, the essence of MIMO radar has not been fully implemented due to the lack of proper transmission waveforms. In MIMO radar, the transmission waveform of each channel has to be uncorrelated with one another to avoid cross-interference between channels. To achieve this, we investigate the generation of uncorrelated multichannel chaos using electrical heterodyning for MIMO chaos radar (MIMO CRADAR) application. By electrically heterodyning a seed chaos source with multiple single-frequency local oscillators, chaos with different heterodyned spectra can be extracted and converted into multiple chaos channels. In this paper, the correlations between different channels of chaos generated are analyzed both numerically and experimentally. The minimal frequency spacing of the local oscillators for generating the largest amount of uncorrelated chaos channels is discussed. In our analysis, thousands of uncorrelated chaos channels can be simultaneously generated with a correlation time of several microseconds. Moreover, compared with those conventional waveform-designing methods that require complicated optimization and digital-to-analog conversion (DAC), the proposed heterodyned technique shows, for the first time, that multiple uncorrelated channels can be generated in real-time while breaking the bandwidth limitation of the DAC devices. A proof-of-concept experiment is successfully demonstrated to show the feasibility of using multichannel heterodyned chaos in the MIMO CRADAR application.

Index Terms: Semiconductor lasers, instabilities and chaos, heterodyne, radar.

1. Introduction

Multiple-input-multiple-output (MIMO) radar has received much attention in recent years for its great imaging performance from the multiplexing capability [1]–[5]. In MIMO radar, several antennas are employed as the transmitters and receivers to simultaneously transmit uncorrelated waveforms and receive their echoes from the target. By transmitting uncorrelated waveform in each channel, the information detected by different pairs of the transmitter and the receiver can be effectively separated. Without ambiguity, snapshots of the target can be obtained. Compared with the synthetic aperture radar (SAR) that requires a mechanical scanning of the transmitter

and the receiver, the MIMO radar provides much higher image acquisition speed. In addition, the effective aperture size of the MIMO radar can be maximized by properly arranging the geometry of the transmitters and the receivers while eliminating the formation of the grating lobes [4], [5]. Therefore, with the same antenna elements used, the MIMO radar can achieve a better spatial resolution than other real aperture radars.

Although the MIMO radar is expected to have the above-mentioned advantages, the essence of MIMO radar is far from being fully implemented. Limited by the slow development in the generation of uncorrelated waveforms, most MIMO radar systems still utilize coherent chirps or short pulses as their transmission waveforms [4], [5]. When using these identical waveforms for all the transmission channels, interleaved transmission and reception are needed and therefore the performance of the MIMO radars is limited. To fully implement the essence of the MIMO radar, the generation of proper uncorrelated waveforms remains to be one of the most crucial issues.

So far, many studies have made efforts to design the suitable waveforms for the application of MIMO radar. Based on the target and clutter statistics, covariance matrix of the transmitted waveforms was designed to control the radiated beam pattern [6], [7]. With power constraints, mutual information between the impulse response of the target and the reflected signal was optimized for waveform selection [8], [9]. Instead of requiring priori knowledge of the target, using code sequences in phase-coded and frequency-coded waveform design was also investigated [10]–[12]. For better orthogonality and signal-to-noise ratio, some optimization algorithms such as simulated annealing and genetic algorithm were utilized to search the code sequences with minimal cross-correlation peaks and peaks of autocorrelation sidelobe [13]–[15]. The methods mentioned above all incorporate complicated optimization processes, which sacrifices and prolongs the computation time in order to generate the demanded waveforms. Under the time constrain in the practical implementation, only limited number and length of the waveforms can be generated with these optimization-based methods.

To increase the degree of freedom on uncorrelated waveform design, generating chaos waveforms using nonlinear dynamical systems has been proposed and studied. Various chaos models were adopted to numerically code the frequency or phase of the modulated signals [16]–[19]. Due to the random nature and the aperiodic property of the chaos, their waveforms inherently possess low cross-correlation peaks and low autocorrelation sidelobe peaks. In addition, the chaos systems are deterministic and very sensitive to the initial conditions. Tuning the initial condition slightly can result in a significant change in the chaos attractors, which can therefore generate a large set of uncorrelated waveforms. More importantly, the generation of chaos waveform is relatively easy. With just a simple iterative computation, chaos waveforms with arbitrary lengths can be efficiently generated for a given initial condition. Nevertheless, digital-to-analog conversions (DAC) are still required for these numerically generated waveforms to be used in the practical transmission. As a consequence, the bandwidths of the transmission waveforms are generally limited by the DAC devices used.

For analog nonlinear dynamical systems, semiconductor lasers and microwave Colpitts oscillators are often adopted to generate chaos waveforms. [20]–[27]. They have been applied in the chaos radar (CRADAR) applications [20]–[23], showing advantages including low probability of intercept, low probability of detection, excellent electronic counter countermeasure, and thumbtack-like ambiguity function [24], [25]. Up to now, most of the chaos radar systems proposed are based on a single chaos channel for one-dimensional ranging [20]–[23]. The implementation of a MIMO chaos radar (MIMO CRADAR) that employs multiple chaos channels has yet to be discussed, however.

To feed the MIMO CRADAR, multiple chaos generation sources with different intrinsic parameters or specially tuned operation conditions can be used to generate multiple uncorrelated chaos waveforms. However, the system could become extremely complex when the number of channel becomes large. To achieve a simple and compact setup for practical implementation, in this study, we propose an electrical heterodyning technique to efficiently generate multiple uncorrelated chaos waveforms using just one single chaos generation source. Since the chaos waveforms generated by semiconductor lasers typically have much broader spectra than those

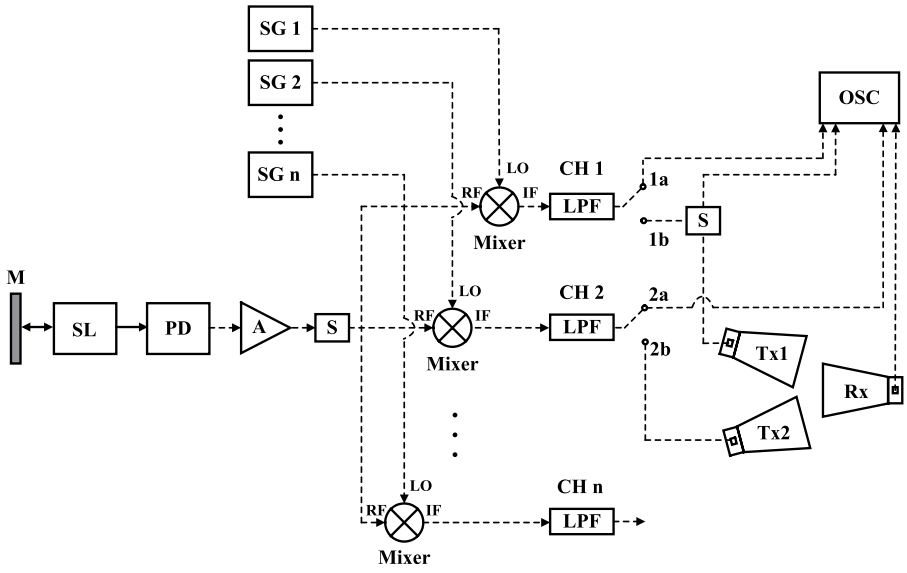

Fig. 1. Schematic setup of the multi-channel chaos generation system based on electrical heterodyning. SL: semiconductor laser; M: mirror; PD: photodetector; A: microwave amplifier; S: microwave splitter; SG: signal generator; LPF: low pass filter; OSC: oscilloscope; Tx and Rx: transmitter and receiver antennas.

generated by microwave Colpitts oscillators [28]–[32], in this study a semiconductor laser subject to optical feedback is used to generate the seed chaos. By electrically heterodyning the seed chaos with multiple local oscillators at different frequencies, the heterodyned chaos waveforms corresponding to different local oscillator frequencies can be simultaneously generated. Similar heterodyne schemes have also been used in suppressing the time delay signature of the chaos [33] and in increasing the bit-rate in random bit generation [34].

In this study, the cross-correlations between the heterodyned chaos waveforms generated with different local oscillation frequencies (f_{LO}) are analyzed both numerically and experimentally. The minimal frequency spacing between each f_{LO} for maximizing the amount of uncorrelated chaos channels is discussed. To show the feasibility of the proposed multi-channel chaos generation in the MIMO CRADAR application, a proof-of-concept experiment is carried out where the cross-interference suppression ratios (CISR) between each heterodyned chaos channel are evaluated.

2. Principle and Numerical Model

The schematic setup of the multi-channel chaos generation system based on electrical heterodyning is shown in Fig. 1. A semiconductor laser subject to optical feedback is utilized as a chaos generator to generate the seed chaos waveform. By adjusting the feedback strength and the feedback delay time for the light reflected from the external mirror, the semiconductor laser can be operated in the chaos oscillation states [32], [35]. The dynamics of the semiconductor laser subject to optical feedback can be modeled by the following coupled rate equations [33], [36], [37]:

$$\frac{da}{dt} = \frac{1}{2}\left[\frac{\gamma_c\gamma_n}{\gamma_s\tilde{J}}\tilde{n} - \gamma_p(2a+a^2)\right](1+a) + \xi\gamma_c[1+a(t-\tau)]\cos[\phi(t-\tau)-\phi(t)] \quad (1)$$

$$\frac{d\phi}{dt} = -\frac{b}{2}\left[\frac{\gamma_c\gamma_n}{\gamma_s\tilde{J}}\tilde{n} - \gamma_p(2a+a^2)\right] + \xi\gamma_c\frac{[1+a(t-\tau)]}{1+a}\sin[\phi(t-\tau)-\phi(t)] \quad (2)$$

$$\frac{d\tilde{n}}{dt} = -\gamma_s\tilde{n} - \gamma_n(1+a)^2\tilde{n} - \gamma_s\tilde{J}(2a+a^2) + \frac{\gamma_s\gamma_p}{\gamma_c}\tilde{J}(2a+a^2)(1+a)^2 \quad (3)$$

where a is the normalized amplitude of the optical field, ϕ is the optical phase, $\tilde{n}$ is the normalized carrier density, ξ is the normalized feedback strength defined as the ratio between the strengths of the reflected field and the emitted field, τ is the feedback delay time, b is the linewidth enhancement factor, $\tilde{J}$ is the normalized bias current, γ_c is the cavity decay rate, γ_n is the differential carrier relaxation rate, γ_s is the spontaneous carrier relaxation rate, and γ_p is the nonlinear carrier relaxation rate. The intrinsic parameters of the laser used, including $b = 3.2$, $\tilde{J} = 1.222$, $\gamma_c = 5.36 \times 10^{11}$ s^{-1}, $\gamma_n = 7.53 \times 10^9$ s^{-1}, $\gamma_s = 5.96 \times 10^9$ s^{-1}, and $\gamma_p = 1.91 \times 10^{10}$ s^{-1}, were experimentally extracted from a single-mode distributed-feedback laser [33], [38].

The laser output is detected by a photodetector and then converted into the electrical signal, which can be represented by its intensity $I(t) = [1 + a(t)]^2$. After amplified by an electrical amplifier, the seed chaos waveform originally generated from the semiconductor laser is then split into different channels. In each channel, a down-converting RF mixer is used to electrically heterodyne the seed chaos with a sinusoidal signal from a signal generator as the local oscillator. In the heterodyne process, the frequency of the local oscillator f_{LO} can be viewed as the axis of symmetry. The portion in the chaos spectrum with frequencies lower than f_{LO} will be flipped up to superpose with those with frequencies higher than f_{LO}. The superposition is then down-shifted toward the dc by a frequency of f_{LO}. Note that, the RF mixer in practical has a finite bandwidth $f_{BW,IF}$ on its output port (IF port). Therefore, the heterodyned chaos generated will only comprise the superposition of the spectra between $f_{LO} - f_{BW,IF}$ and $f_{LO} + f_{BW,IF}$. To prevent any possible leakage of the input signal through the RF mixers in the high frequency region due to imperfect isolation, low-pass filters having the same bandwidth as the RF mixer are used. An oscilloscope is then used to acquire the heterodyned chaos waveforms generated. By applying multiple local oscillators with different f_{LO} to extract and superpose different portions of the seed chaos spectrum, multiple channels of heterodyned chaos can be simultaneously generated.

To simplify the analysis, only two channels are employed in our setup for proof-of-concept demonstration. The heterodyned chaos signals obtained in channel 1 (CH1) and channel 2 (CH2) through the direct connections of points 1a and 2a as shown in Fig. 1 can be represented by

$$S_{CH1}(t) = \mathrm{LPF}[I(t) \times \cos(2\pi f_{LO1} t)] \tag{4}$$

$$S_{CH2}(t) = \mathrm{LPF}[I(t) \times \cos(2\pi f_{LO2} t)] \tag{5}$$

where LPF$[\cdot]$ is a low-pass filter with a –3 dB bandwidth of $f_{BW,IF}$. A uniform frequency response is assumed. (4) and (5) can be further derived as

$$S_{CH1}(t) = \int_{\omega_{LO1}}^{\omega_{LO1}+\omega_{BW,IF}} A(\omega)\cos[(\omega - \omega_{LO1})t + \phi(\omega)]d\omega + \int_{\omega_{LO1}-\omega_{BW,IF}}^{\omega_{LO1}} A(\omega)\cos[(\omega_{LO1} - \omega)t - \phi(\omega)]d\omega \tag{6}$$

$$S_{CH2}(t) = \int_{\omega_{LO2}}^{\omega_{LO2}+\omega_{BW,IF}} A(\omega)\cos[(\omega - \omega_{LO2})t + \phi(\omega)]d\omega + \int_{\omega_{LO2}-\omega_{BW,IF}}^{\omega_{LO2}} A(\omega)\cos[(\omega_{LO2} - \omega)t - \phi(\omega)]d\omega \tag{7}$$

where $A(\omega)$ and $\phi(\omega)$ are the amplitude spectrum and phase spectrum of the seed chaos, and ω_{LO1}, ω_{LO2}, and $\omega_{BW,IF}$ are the angular frequencies of f_{LO1}, f_{LO2}, and $f_{BW,IF}$, respectively. By considering the general characteristics of the seed chaos obtained from (1)–(3), $A(\omega)$ with a bandwidth much broader than twice of the $f_{BW,IF}$ and $\phi(\omega)$ with a random phase relation in different frequencies are assumed in our theoretical analysis. When the frequency difference of f_{LO1} and f_{LO2} ($|\Delta f = \Delta\omega/2\pi| = |f_{LO2} - f_{LO1}|$) is larger than twice of the $f_{BW,IF}$ ($|\Delta f| > 2f_{BW,IF}$), the heterodyned chaos in CH1 and CH2 are extracted from different portions of the seed chaos spectrum that are completely not overlapped. Therefore, $S_{CH1}(t)$ and $S_{CH2}(t)$ will be uncorrelated since there is no particular phase relation among different frequency components in the seed chaos spectrum. In this case, the largest number of uncorrelated chaos channels one can extract from a seed chaos

is estimated to be $(f_{BW,chaos} - 2f_{BW,IF})/2f_{BW,IF}$, where $f_{BW,chaos}$ is the bandwidth of the seed chaos provided.

To squeeze out more of the uncorrelated chaos channels from the seed chaos, setting $|\Delta f|$ below $f_{BW,IF}$ is demanded. When f_{LO2} is very close to f_{LO1} ($|\Delta f| \ll f_{BW,IF}$), (6) and (7) can be expanded as

$$S_{CH1}(t) = \int_{\omega_{LO1}}^{\omega_{LO2}} A(\omega)\cos[(\omega-\omega_{LO1})t + \phi(\omega)]d\omega + \int_{\omega_{LO2}}^{(\omega_{LO2}+\omega_{BW,IF})-\Delta\omega} A(\omega)\cos[(\omega-\omega_{LO1})t + \phi(\omega)]d\omega + \int_{\omega_{LO1}-\omega_{BW,IF}}^{(\omega_{LO1}-\omega_{BW,IF})+\Delta\omega} A(\omega)\cos[(\omega_{LO1}-\omega)t - \phi(\omega)]d\omega + \int_{(\omega_{LO1}-\omega_{BW,IF})+\Delta\omega}^{\omega_{LO1}} A(\omega)\cos[(\omega_{LO1}-\omega)t - \phi(\omega)]d\omega \tag{8}$$

$$S_{CH2}(t) = \int_{(\omega_{LO2}+\omega_{BW,IF})-\Delta\omega}^{\omega_{LO2}+\omega_{BW,IF}} A(\omega)\cos[(\omega-\omega_{LO2})t + \phi(\omega)]d\omega + \int_{\omega_{LO2}}^{(\omega_{LO2}+\omega_{BW,IF})-\Delta\omega} A(\omega)\cos[(\omega-\omega_{LO2})t + \phi(\omega)]d\omega + \int_{\omega_{LO1}}^{\omega_{LO2}} A(\omega)\cos[(\omega_{LO2}-\omega)t - \phi(\omega)]d\omega + \int_{(\omega_{LO1}-\omega_{BW,IF})+\Delta\omega}^{\omega_{LO1}} A(\omega)\cos[(\omega_{LO2}-\omega)t - \phi(\omega)]d\omega. \tag{9}$$

Under this condition of $|\Delta f| \ll f_{BW,IF}$, as shown in (8) and (9), the spectral power extracted by $S_{CH1}(t)$ and $S_{CH2}(t)$ are now from partially overlapped portions of the seed chaos spectrum. To ensure that the heterodyned chaos generated under this condition are still highly uncorrelated, the cross-correlations defined as

$$\rho(\tau) = \int_{T_i}^{T_i+T_{corr}} S_{CH1}(t)S_{CH2}(t-\tau)dt \tag{10}$$

among each channel are evaluated [4], [10], [14], [16]. The T_i and T_{corr} in the temporal integral are the initial integration time and the correlation time, respectively. Since the heterodyned chaos waveforms in each channel are originated and extracted from the same seed chaos, their cross-correlation is most likely to peak around the zero-lag time provided that there is any correlation among them. By taking (8) and (9) into (10), the cross-correlation of $S_{CH1}(t)$ and $S_{CH2}(t)$ at zero-lag becomes

$$\rho(0) = \int_{T_i}^{T_i+T_{corr}} \left\{ \iint_{\omega_{LO2}}^{(\omega_{LO2}+\omega_{BW,IF})-\Delta\omega} A(\omega)A(\omega')\cos[(\omega-\omega'+\omega_{LO2}-\omega_{LO1})t + \phi(\omega) - \phi(\omega')]d\omega d\omega' + \iint_{(\omega_{LO1}-\omega_{BW,IF})+\Delta\omega}^{\omega_{LO1}} A(\omega)A(\omega')\cos[(\omega-\omega'+\omega_{LO2}-\omega_{LO1})t + \phi(\omega) - \phi(\omega')]d\omega d\omega' + \iint_{\omega_{LO1}}^{\omega_{LO2}} A(\omega)A(\omega')\cos[(\omega+\omega'-\omega_{LO2}-\omega_{LO1})t + \phi(\omega) + \phi(\omega')]d\omega d\omega' + \text{cross-products from non-overlapped spectra} \right\} dt. \tag{11}$$

Since the seed chaos has a random relation in $\phi(\omega)$, the cross-products of $S_{CH1}(t)$ and $S_{CH2}(t)$ can only be coherently superposed at $\omega = \omega'$ when having a fixed phase relation. The

incoherent cross-products from $\omega \neq \omega'$ will in contrast have a random phase variation with time, which will be averaged out after a certain length of T_{corr}. Therefore, by ignoring the effect from those incoherent products (including those cross-products from the non-overlapped spectra), (11) can be approximated as

$$\begin{aligned}\rho(0) &\approx \int_{T_i}^{T_i+T_{corr}} \left\{ \int_{\omega_{LO2}}^{(\omega_{LO2}+\omega_{BW,IF})-\Delta\omega} A^2(\omega)\cos[(\omega_{LO2}-\omega_{LO1})t]d\omega \right. \\ &\qquad \left. + \int_{(\omega_{LO1}-\omega_{BW,IF})+\Delta\omega}^{\omega_{LO1}} A^2(\omega)\cos[(\omega_{LO2}-\omega_{LO1})t]d\omega \right\} dt \\ &= C\left[\int_{T_i}^{T_i+T_{corr}} \cos(\Delta\omega t)dt\right] \\ &= \frac{C}{\Delta\omega}\{\sin(\Delta\omega T_{corr})\cos(\Delta\omega T_i) + [\cos(\Delta\omega T_{corr})-1]\sin(\Delta\omega T_i)\} \end{aligned} \tag{12}$$

where the constant $C = \int_{\omega_{LO2}}^{(\omega_{LO2}+\omega_{BW,IF})-\Delta\omega} A^2(\omega)d\omega + \int_{(\omega_{LO1}-\omega_{BW,IF})+\Delta\omega}^{\omega_{LO1}} A^2(\omega)d\omega$.

As can be seen in (12), for those heterodyned chaos extracted with Δf equal to the integer multiples of $1/T_{corr}$ ($\Delta f = \Delta\omega/2\pi = m \cdot 1/T_{corr}, m = 1, 2, 3, \ldots$), $|\rho(0)|$ between each channel will have minima, regardless of T_i. In contrast, for those heterodyned chaos extracted with Δf not equal to the integer multiples of $1/T_{corr}$ ($\Delta f \neq m \cdot 1/T_{corr}, m = 1, 2, 3, \ldots$), $|\rho(0)|$ between the channels could vary significantly depending on $\Delta\omega$, T_{corr}, and T_i. Therefore, when $|\Delta f| \ll f_{BW,IF}$, the largest number of uncorrelated chaos channels that can be simultaneously generated from a single seed chaos is estimated as $(f_{BW,chaos} - 2f_{BW,IF})/(1/T_{corr})$, where $\Delta f = 1 \cdot 1/T_{corr}$ is the minimal frequency spacing between the local oscillators for $|\rho(0)|$ to be minimized. By increasing T_{corr}, the minimal frequency spacing can be reduced and hence the number of uncorrelated chaos channels can be increased as long as the Δf chosen still satisfy the condition of $\Delta f = m \cdot 1/T_{corr}, m = 1, 2, 3, \ldots$.

Note that (12) is only valid when the seed signal has a broad bandwidth in $A(\omega)$ and a random relation in $\phi(\omega)$ as those in the chaos waveforms. For other seed signals with relatively small bandwidths in $A(\omega)$ or having some particular relation in $\phi(\omega)$, the incoherent cross-products from different frequencies ($\omega \neq \omega'$) will in general not be averaged out and correlations between channels will be present.

3. Simulation Results

In the numerical analysis, the seed chaos is generated by solving (1)–(3) with a second-order Runge-Kutta integration. The integration is conducted with a time step of 1 ps for a duration over 100 μs. The finite bandwidth on the output port of the down-converting RF mixer is numerically implemented by a Chebyshev Type-II low pass filter with an $f_{BW,IF} = 4$ GHz. With a feedback strength $\xi = 0.09$ and a feedback delay time $\tau = 5$ μs, the power spectrum of the seed chaos generated is shown in Fig. 2(a). Here a relatively long delay in the feedback is chosen to obtain a broad and continuous chaos spectrum. This seed chaos has a standard chaos bandwidth of 16 GHz, which measures the central portion of the frequency span where 80% of the total power is contained within [39]. After heterodyning with an f_{LO} of 4 GHz, the power spectrum, time series, and the auto-correlation trace of the heterodyned chaos generated are shown in Fig. 2(b)–(d), respectively. As can be seen, the power spectrum of the heterodyned chaos is flat and smooth; the time series shows a noise-like waveform without periodicity; and in the auto-correlation trace, no significant peak and meaningful feature can be observed, except for the mainlobe, respectively. Inheriting the chaotic nature from the seed chaos, the heterodyned chaos is expected to preserve the essential properties for the CRADAR applications [20], [24].

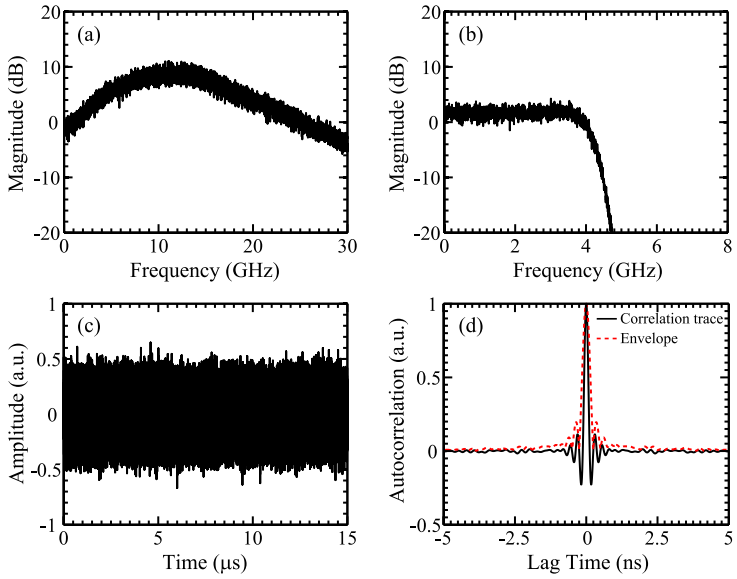

Fig. 2. (a) Power spectrum of the seed chaos obtained numerically with a feedback strength $\xi = 0.09$ and a feedback delay time $\tau = 5$ μs. (b) Power spectrum, (c) time series, and (d) autocorrelation function of the heterodyned chaos obtained numerically by electrically heterodyning the seed chaos in (a) with an $f_{LO} = 4$ GHz.

The correlations between heterodyned chaos channels obtained with different local oscillation frequencies are analyzed in Fig. 3, where f_{LO1} is fixed at 4 GHz while f_{LO2} is varied to have different Δf. The dependence of the correlation on T_i is also discussed. The black curves in Fig. 3(a)–(j) show the zero-lag cross-products and the normalized cross-correlations of the heterodyned chaos with $T_{corr} = 5$ μs, respectively. The red dashed curves in Fig. 3(f)–(j) show the envelopes of the cross-correlation traces $\rho_e(\tau)$ obtained through Hilbert transform. When $f_{LO2} = 12$ GHz $(\Delta f = 8$ GHz$)$, the two heterodyned chaos are uncorrelated because they are extracted from portions of the seed chaos spectrum that are completely not overlapped. As shown in Fig. 3(a), the zero-lag cross-product shows a random amplitude fluctuation resulting from the incoherent spectral relation between the chaos channels. Accordingly, no meaningful peak is present in the cross-correlation trance shown in Fig. 3(f). Under this condition, the amplitudes of the cross-correlation at the zero-lag time are essentially zero independent of T_i.

To squeeze out more of the uncorrelated chaos channels from the seed chaos, setting $|\Delta f|$ below $f_{BW,IF}$ is demanded. When reducing Δf, the coherent product between the heterodyned chaos channels becomes dominant. Together with the random variation originating from the incoherent product, a sinusoidal modulation having a frequency of Δf starts to be revealed in the trace of the zero-lag cross-product. In this case, the initial integration phase $(\phi_i = \Delta\omega \times T_i)$ determined by T_i has a strong influence on the cross-correlation as described in (12). When $\Delta f = 0.3$ MHz $(f_{LO2} = 4.0003$ GHz$)$ and $\phi_i = 1.5\pi$ and 2π, as shown in Fig. 3(b) and (c), the sinusoidal modulation from the coherent product has 1.5 periods within T_{corr} of 5 μs. For $\phi_i = 1.5\pi$, the cross-correlation as shown in Fig. 3(g) has a large amplitude at the zero-lag time. For $\phi_i = 2\pi$, although the amplitude of the cross-correlation in Fig. 3(h) happens to be zero at the exact zero-lag time, the obvious sidelobes on both sides of zero-lag time indicate the existence of the cross-interference. Here, by taking the envelope detection (red dashed curves), a non-zero cross-correlation envelope $\rho_e(0)$ at the zero-lag time is clearly identified.

When Δf is reduced to 0.2 MHz $(f_{LO2} = 4.0002$ GHz$)$, the sinusoidal modulations will have exactly one full-period within T_{corr} of 5 μs as shown in Fig. 3(d) and (e) for $\phi_i = 1.5\pi$ and 2π, respectively. Since integrating a full-period of sinusoidal waveform is always equal to zero independent of ϕ_i, the amplitudes of the cross-correlations for $\phi_i = 1.5\pi$ and 2π as shown in Fig. 3(i) and (j) respectively are therefore essentially zero at the zero-lag time. In these cases,

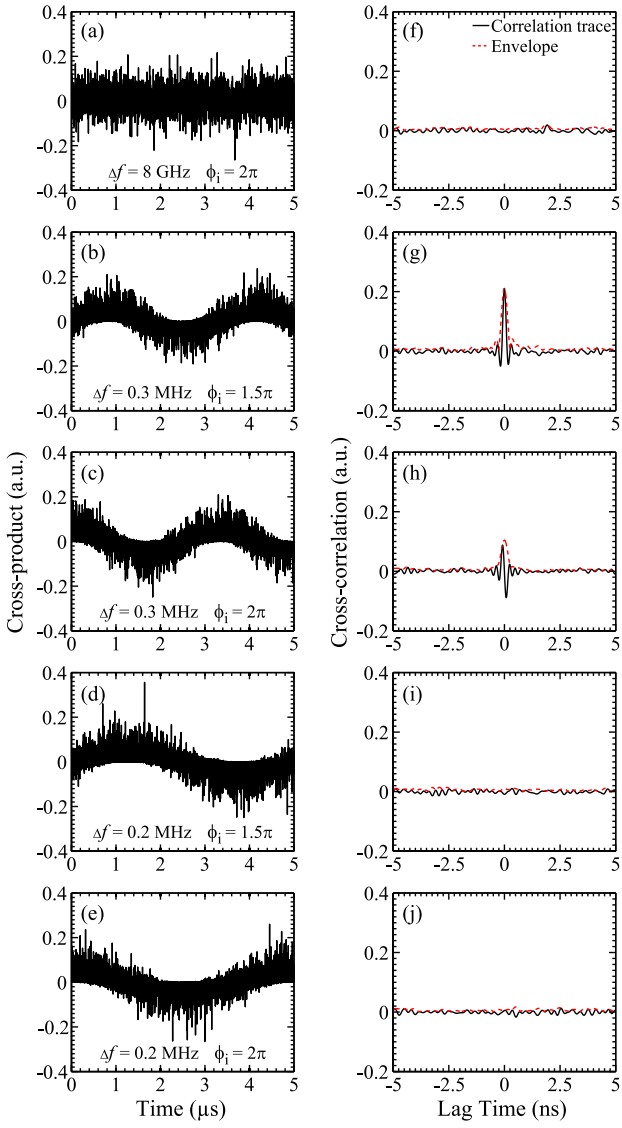

Fig. 3. (a)–(e) Zero-lag cross-product and (f)–(j) normalized cross-correlation between the heterodyned chaos obtained with an $f_{LO1} = 4$ GHz and $f_{LO2} = 12$ GHz (first row), 4.0003 GHz (second and third rows), and 4.0002 GHz (fourth and fifth rows). The initial integration phase $\phi_i = 2\pi$ in the first, third, and fifth rows, and $\phi_i = 1.5\pi$ in second and fourth rows.

both the coherent and incoherent products are averaged out. From the results shown, even when extracting the heterodyned chaos from largely overlapped portions of the chaos spectrum to maximize the number of uncorrelated channels, the correlation between channels can still be kept at the same minimal level thanks to the nature of the broad bandwidth and random phase of chaos.

To quantify the correlations between different heterodyned chaos channels generated under different Δf, amplitudes of cross-correlation envelopes $\rho_e(0)$ at the zero-lag time are analyzed. Fig. 4(a) and (b) show the $\rho_e(0)$ between the chaos channels for different normalized Δf ($\Delta \tilde{f} = |\Delta f| \times T_{corr}$) under T_{corr} of 2.5 μs and 5 μs, respectively. Here, $\rho_e(0)$ for each Δf are averaged over 50 different time sequences from the chaos waveforms. The green dotted lines are the background noise calculated from the average amplitude of the $\rho_e(\tau)$ excluding the mainlobe showing the baselines of $\rho_e(0)$. As can be seen, $\rho_e(0)$ in Fig. 4(a) and (b) show the same variation trend where $\rho_e(0)$ tends to converge to zero with a periodic oscillation. Note that similar

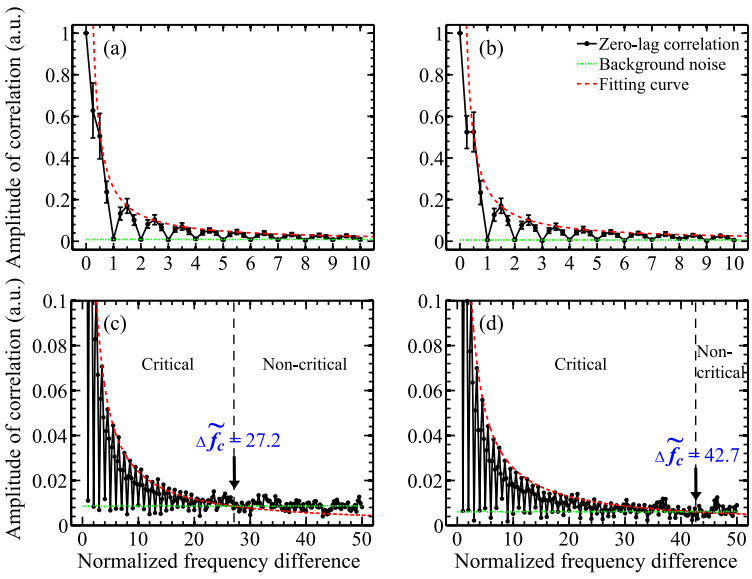

Fig. 4. $\rho_e(0)$ between chaos channels obtained numerically for different $\Delta\tilde{f}$ under (a) $T_{corr} = 2.5$ μs and (b) $T_{corr} = 5$ μs, respectively. (c) and (d) Enlargement of (a) and (b), respectively. The green dotted lines show the background noise of the cross-correlation traces. The red dashed curves show the fitting curves of $\rho_e(0)$ at $\Delta\tilde{f} = m - 0.5$.

trends are observed for different T_{corr}, which is also independent with the relation between the feedback delay time τ and T_{corr}.

For $\Delta\tilde{f} = m$ $(m = 1, 2, 3, \ldots)$, $\rho_e(0)$, which is comparable to the background noise level, can be obtained. On the contrary, for $\Delta\tilde{f} = m - 0.5$, $\rho_e(0)$ has its local maxima. Resulting from the strong dependence of $\rho_e(0)$ on ϕ_i, the standard deviations of those from $\Delta\tilde{f} = m - 0.5$ are also larger than those obtained from $\Delta\tilde{f} = m$. Although $\rho_e(0)$ is large when $\Delta\tilde{f}$ is small, the local maxima of $\rho_e(0)$ at $\Delta\tilde{f} = m - 0.5$ gradually decrease and submerge into the background noise as $\Delta\tilde{f}$ increases. The red dashed curves shown in Fig. 4(a) and (b) are the polynomial fitting of those local maxima of $\rho_e(0)$ at $\Delta\tilde{f} = m - 0.5$. As can be seen, the local maxima are inversely proportional to $\Delta\tilde{f}$, which is also predicted by the formula derived in (12).

To show the details of $\rho_e(0)$ as $\Delta\tilde{f}$ further increases, Fig. 4(c) and (d) show $\rho_e(0)$ for different $\Delta\tilde{f}$, similar to those in Fig. 4(a) and (b), but with a wider range of $\Delta\tilde{f}$ and a finer scale of $\rho_e(0)$ just above 0. Similarly, the green dotted lines and the red dashed curves are the background noise and the fitting of the local maxima, respectively. As can be seen, before those local maxima submerge into the background noise at $\Delta\tilde{f}_c$ indicated by the black arrows shown in Fig. 4(c) and (d), the choice the local oscillation frequencies is very critical. Uncorrelated heterodyned chaos can only be generated when $\Delta\tilde{f}$ is an integer so that $\rho_e(0)$ has its minimum. On the contrary, the choice the local oscillation frequencies becomes non-critical when $\Delta\tilde{f} > \Delta\tilde{f}_c$ since all $\rho_e(0)$ are already small and have submerged into the background noise, regardless of whether $\Delta\tilde{f}$ is an integer or a half-integer.

In other words, to generate multi-channel chaos with low cross-correlations, $\Delta\tilde{f}$ has to be an integer in the critical operation region $(\Delta\tilde{f} < \Delta\tilde{f}_c)$ while it can be arbitrary in the non-critical operation region $(\Delta\tilde{f} > \Delta\tilde{f}_c)$. Hence, the minimal frequency spacing between the local oscillators for multi-channel chaos generations is when $\Delta\tilde{f} = 1$ in the critical operation region and is $\Delta\tilde{f}_c$ in the non-critical operation region, respectively. For a seed chaos with a given bandwidth, these minimal frequency spacings determine the largest numbers of uncorrelated chaos channels that can be simultaneously generated. For $\Delta\tilde{f}_c = 27.2$ and $\Delta\tilde{f}_c = 42.7$ in the cases of

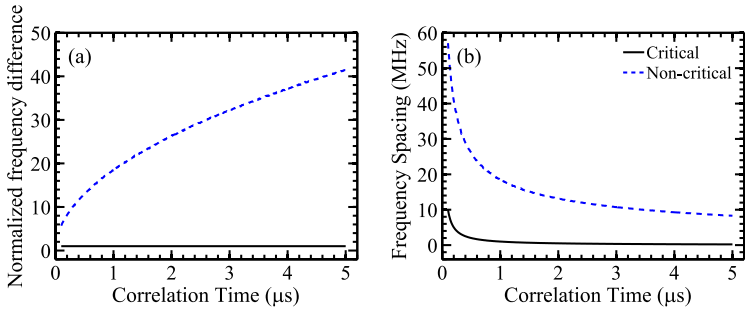

Fig. 5. (a) Minimal $\Delta\tilde{f}$ and (b) minimal Δf under critical (black solid curves) and non-critical (blue dashed curves) operation regions for different T_{corr}.

$T_{corr} = 2.5\ \mu$s and $T_{corr} = 5\ \mu$s, as shown in Fig. 4(c) and (d), respectively, the corresponding minimal frequency spacings are 10.9 MHz and 8.5 MHz for the non-critical operation cases. For the critical operation, the minimal frequency spacings are 0.4 MHz and 0.2 MHz for T_{corr} of 2.5 μs and 5 μs, respectively.

Based on (12) and the same numerical analysis as that used in Fig. 4 to obtain the fitting curves and background noise under different T_{corr}, Fig. 5(a) shows the minimal $\Delta\tilde{f}$ for different T_{corr} under the non-critical (blue dashed curve) and critical (black solid curve) operations, respectively. The corresponding minimal frequency spacings are shown in Fig. 5(b). As can be seen, for the non-critical operation, the minimal $\Delta\tilde{f}$ $(= \Delta\tilde{f}_c)$ monotonically increases as T_{corr} increases. This is due to the lower background noise associated with the longer T_{corr}, which intersects with the local maxima of $\rho_e(0)$ at larger $\Delta\tilde{f}$ as those shown in Fig. 4(c) and (d). However, the decrease in $1/T_{corr}$ is faster than the increase of $\Delta\tilde{f}$ as T_{corr} increases. Therefore, as shown in Fig. 5(b), the minimal frequency spacing is still dominated by $1/T_{corr}$ and monotonically decreases as the T_{corr} increases. This minimal frequency spacing decreases rapidly and gradually converges to about 10 MHz after several microseconds.

For the critical operation, the minimal $\Delta\tilde{f}$ is always 1 for all T_{corr}. Therefore, the corresponding minimal frequency spacing is exactly inversely proportional to T_{corr}. For a T_{corr} of serval μs, the minimal frequency spacing can be reduced to below 1 MHz. From the analysis, with $f_{BW,chaos} =$ 16 GHz and $f_{BW,IF} = 4$ GHz as those used in the simulation, the numbers of uncorrelated chaos channels that can be simultaneously generated under the non-critical and critical operation regions are estimated to be about 800 $((16\ \text{GHz} - 4\ \text{GHz} \times 2)/10\ \text{MHz})$ and 8000 $((16\ \text{GHz} - 4\ \text{GHz} \times 2)/1\ \text{MHz})$ for a T_{corr} of several μs. As can be seen, having a smaller minimal frequency spacing, more number of chaos channels can be generated in general when operating in the critical operation region than in the non-critical operation region. However, it in contrast requires much better control in the frequency precision and the stability of the local oscillation frequencies so that $\rho_e(0)$ can maintain at its local minimum over time.

4. Experimental Results

To show the feasibility, a multi-channel chaos generation system based on the electrical heterodyning is implemented. The source of the chaos signal is generated by a single-mode distributed-feedback semiconductor laser subject to optical feedback. With a normalized feedback strength of 0.26 and a feedback delay time of 5 μs, the laser can be operated in a chaos state with a broad and flat spectrum. The chaotic light is detected by a 12 GHz high-speed photodetector (Newport 1554-A) and converted to the electrical signal, namely, the seed chaos. The seed chaos is then amplified by a broadband amplifier (Miteq AFS6-00102000-30) with a gain of about 30 dB and a 3 dB passband between 0.1–20 GHz. With a microwave splitter, the amplified seed chaos is divided into two channels for demonstration. In each channel, the seed chaos is electrically heterodyned with a sinusoidal signal through a down-converting RF mixer (Mini-Circuits ZX05-153MH+) that has RF and LO passbands between 3.2–15 GHz and an IF

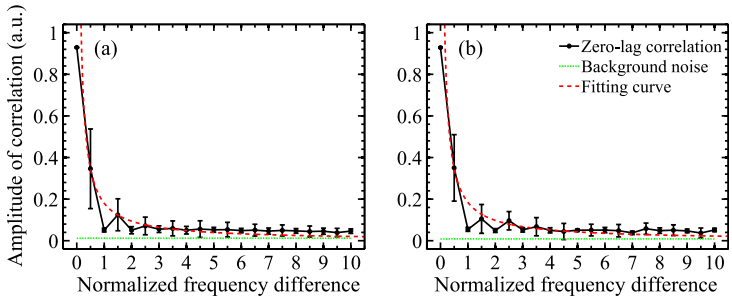

Fig. 6. $\rho_e(0)$ between chaos channels obtained experimentally for different $\Delta\tilde{f}$ under (a) $T_{corr} = 2.5\ \mu$s and (b) $T_{corr} = 5\ \mu$s, respectively. The green dotted lines show the background noise of the cross-correlation traces. The red dashed curves show the fitting curves of $\rho_e(0)$ at $\Delta\tilde{f} = m - 0.5$.

passband between DC-4 GHz. After electrically heterodyned with the sinusoidal signals generated from two signal generators (Angilent E4422B and Anritsu MG3692B) as the local oscillators, the heterodyned chaos pass through low-pass filters (Mini-Circuits VLF-3400+) with a passband of DC-4 GHz for suppressing the unwanted power leakage of the RF mixer in the high-frequency region. Finally, the heterodyned chaos in CH1 and CH2 are simultaneously acquired by an oscilloscope (Tektronix TDS6604) that has a bandwidth of 6 GHz and a sampling rate of 20 GS/s. The time duration of each acquisition is 10 μs. To have the similar operation condition as those used in the simulation, the f_{LO1} is fixed at 4 GHz, while the f_{LO2} is varied to calculate $\rho_e(0)$ with different Δf.

Fig. 6(a) and (b) show $\rho_e(0)$ between the chaos obtained experimentally in CH1 and CH2 for different $\Delta\tilde{f}$ under T_{corr} of 2.5 μs and 5 μs, respectively. Similar to the variations seen in Fig. 4(a) and (b), the $\rho_e(0)$ in Fig. 6(a) and (b) also oscillate periodically and tend to converge as $\Delta\tilde{f}$ increases. The correlations between the two chaos channels are again low at $\Delta\tilde{f} = m$ and high at $\Delta\tilde{f} = m - 0.5$. Although LPFs are used to reject the direct power leakage for frequencies higher than the bandwidth of the mixer, the leakage within the bandwidth of the RF mixer still cannot be avoided. As the results, due to the imperfect isolation of the RF mixer, the baselines of the $\rho_e(0)$ are slightly elevated from the background noise (green dotted lines) in experiments as shown in Fig. 6(a) and (b). In addition, the local maxima of $\rho_e(0)$ at $\Delta\tilde{f} = m - 0.5$ (as well as their fitting in the red dashed curves) have slightly smaller correlation amplitudes compared with the simulation results shown in Fig. 4. For one of the most obvious case, the $\rho_e(0)$ between the heterodyned chaos generated from exactly the same f_{LO} ($\Delta\tilde{f} = 0$) has dropped to 0.93 from the ideal value of 1. This lowering in $\rho_e(0)$ is mainly due to the unwanted noise coupled into the channels and the finite analog-to-digital sampling rate in the oscilloscope.

As demonstrated in the experiment, uncorrelated chaos can be again generated when $\Delta\tilde{f} = m$ in the critical operation region or for any arbitrary $\Delta\tilde{f}$ in the non-critical operation region. Note that, having lower $\rho_e(0)$, higher background noise, and higher baseline of $\rho_e(0)$, the $\Delta\tilde{f}_c$ obtained experimentally are lower than those found in the simulation when under the same condition. In other words, more uncorrelated chaos channels can actually be simultaneously generated in practical implementations attributes to the noise inevitably coupled into the channels.

5. Proof-of-Concept Demonstration

To demonstrate the feasibility of the MIMO CRADAR application, a proof-of-concept experiment using the multi-channel chaos generated is carried out. The setup is similar to the one shown in Fig. 1, but now the outputs of CH1 and CH2 are connected to the respective points of 1b and 2b to include the effects from the antennas. The heterodyned chaos in CH1 is split into a reference signal and a probe signal. The probe signal is transmitted (Tx1) and then received (Rx) by a pair of broadband horn antennas (A-INFO LB10180) that have passbands

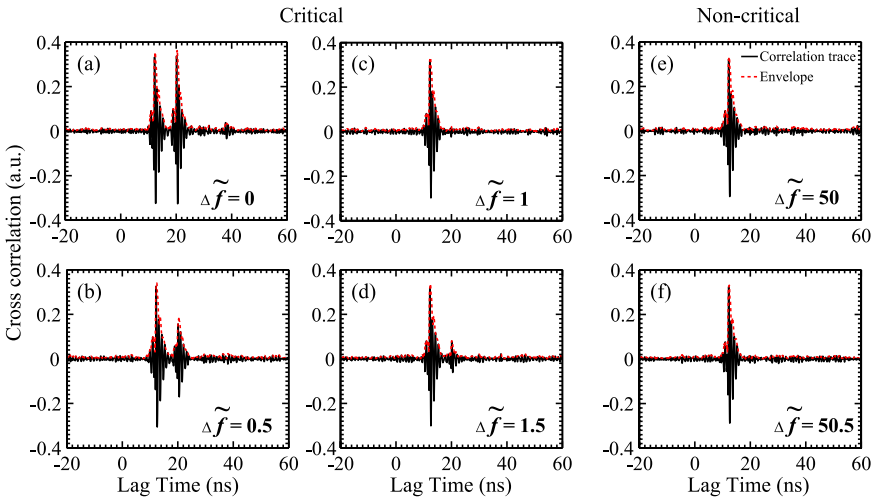

Fig. 7. Cross-correlation traces between the received signals and the reference signals when two transmitted chaos channels having (a) $\Delta\tilde{f} = 0$, (b) $\Delta\tilde{f} = 0.5$, (c) $\Delta\tilde{f} = 1$, (d) $\Delta\tilde{f} = 1.5$, (e) $\Delta\tilde{f} = 50$, and (f) $\Delta\tilde{f} = 50.5$, respectively.

between 1–18 GHz. The heterodyned chaos in CH2 is also transmitted with another similar antenna (Tx2) and received by the Rx to simulate the co-existence of multiple channels in the MIMO CRADAR environment. The reference signal in CH1 and the signal received by the Rx are simultaneously recorded with the oscilloscope.

For T_{corr} of 5 μs, Fig. 7(a)–(f) show the cross-correlation traces between the received signals and the reference signals for $\Delta\tilde{f} = 0$, 0.5, 1, and 1.5 in the critical operation cases and $\Delta\tilde{f} = 50$ and 50.5 in the non-critical operation cases, respectively. The red dashed curves are their envelopes calculated by the Hilbert transform. To quantify the cross-interference between the channels, a cross-interference suppression ratio (CISR) defined by the amplitude ratio between the main (first) and the side (second) peaks in the envelope of the cross-correlation trace is calculated. As can be seen in Fig. 7(a), when there is no frequency difference in the f_{LO} between CH1 and CH2 $(\Delta\tilde{f} = 0)$, the chaos from CH1 and CH2 are identical and therefore two distinct peaks with almost equal amplitudes are observed. The lag times of the peaks are corresponding to the path lengths in CH1 and CH2, and the relative time delay between these peaks is corresponding to the path difference between the Tx1 and Tx2 to the Rx. When $\Delta\tilde{f}$ is increased to 0.5 as shown in Fig. 7(b), the cross-interference from CH2 is reduced where the side peak is lowered in its amplitude. For $\Delta\tilde{f} = 1$ as shown in Fig. 7(c), the side peak corresponding to the cross-interference from CH2 vanishes completely. Under this condition, the chaos from CH1 and CH2 are shown to be uncorrelated to each other. Further increasing $\Delta\tilde{f}$ to 1.5 as shown in Fig. 7(d) increases the amplitude of the side peak again. The CISR for $\Delta\tilde{f} = 0$, 0.5, 1, and 1.5 in these critical operation cases are calculated to be –0.1, 3.1, 15.1, and 6.3 dB, respectively. As expected, a large CISR is obtained only when $\Delta\tilde{f}$ is an integer in the critical operation region.

In contrast, in the non-critical operation region, the CISR maintains at a similar level for all different $\Delta\tilde{f}$ no matter it is an integer or a half-integer. As shown in Fig. 7(e) and (f), the CISR for $\Delta\tilde{f} = 50$ and 50.5 are 14.8 and 14.9 dB, respectively. Note that the highest CISR in the current setup is about 15 dB, which is limited by the imperfect isolation of the RF mixers used.

6. Conclusion

In this study, we investigate the generation of multi-channel chaos using electrical heterodyning for MIMO CRADAR application. By electrically heterodyning a seed chaos with multiple

single-frequency local oscillators, different portions of the chaos spectrum are extracted and converted into different chaos channels. By carefully selecting the frequency difference of the local oscillators, heterodyned chaos with uncorrelated waveforms can be generated. The critical and non-critical operation regions are defined and identified. In the critical operation region, the uncorrelated chaos can be obtained only when $\Delta\tilde{f}$ is an integer. In the non-critical operation region, $\Delta\tilde{f}$ can be chosen arbitrarily. The minimal frequency spacing between channels is found to be determined by T_{corr} in both operation regions. By increasing T_{corr}, the minimal frequency spacing can be reduced in order to produce more uncorrelated chaos channels. From our analysis, for T_{corr} of several μs, thousands of uncorrelated chaos channels can be generated simultaneously. To the best of our knowledge, this is the largest number of uncorrelated waveforms with infinite lengths that can be simultaneously generated up-to-date. Moreover, compared with those waveform-designing methods which require complicated optimization and DAC process [6]–[18], generation of multi-channel chaos with the proposed heterodyne scheme can be in real-time and break the bandwidth limitation of the DAC devices. The proof-of-concept experiment successfully demonstrates the feasibility of the heterodyned chaos for the MIMO CRADAR application, where excellent CISR with minimum ambiguity in target detection is achieved.

It is also worth mentioning that, since the heterodyned chaos can be easily switched from completely uncorrelated to highly correlated by varying $\Delta\tilde{f}$ from an integer to a half-integer in the critical operation region, a multi-function radar array that integrates both the advantages of a MIMO CRADAR and a timed-array radar can potentially be realized based on this heterodyne technique. With the MIMO CRADAR, applications in the fields of geophysical and terrestrial imaging, area surveillance, unmanned aircraft and vehicle, target search, track, and missile guidance for warships could all be realized.

References

[1] E. Fishler *et al.*, "MIMO radar: An idea whose time has come," in *Proc. IEEE Radar Conf.*, 2004, pp. 71–78.
[2] J. Li and P. Stoica, "MIMO radar with colocated antennas," *IEEE Signal Process. Mag.*, vol. 24, no. 5, pp. 106–114, Sep. 2007.
[3] D. W. Bliss and K. W. Forsythe, "Multiple-Input Multiple-Output (MIMO) radar and imaging: Degrees of freedom and resolution," in *Conf. Rec. 37th Asilomar Conf. Signals, Syst. Comput.*, 2004, pp. 54–59.
[4] D. Tarchi, F. Oliveri, and P. F. Sammartino, "MIMO radar and ground-based SAR imaging systems: Equivalent approaches for remote sensing," *IEEE Trans. Geosci. Remote Sens.*, vol. 51, no. 1, pp. 425–435, Jan. 2013.
[5] X. Zhuge and A. G. Yarovoy, "A sparse aperture MIMO-SAR-based UWB imaging system for concealed weapon detection," *IEEE Trans. Geosci. Remote Sens.*, vol. 49, no. 1, pp. 509–518, Jan. 2011.
[6] D. R. Fuhrmann and G. S. Antonio, "Transmit beamforming for MIMO radar systems using partial signal correlation," in *Conf. Rec. 38th Asilomar Conf. Signals, Syst. Comput.*, 2004, pp. 295–299.
[7] P. Stoica, J. Li, and Y. Xie, "On probing signal design for MIMO radar," *IEEE Trans. Signal Process.*, vol. 55, no. 8, pp. 4151–4161, Aug. 2007.
[8] Y. Yang and R. S. Blum, "MIMO radar waveform design based on mutual information and minimum mean-square error estimation," *IEEE Trans. Aerosp. Electron. Syst.*, vol. 43, no. 1, pp. 330–343, Jan. 2007.
[9] Y. Yang and R. S. Blum, "Minimax robust MIMO radar waveform design," *IEEE J. Sel. Topics Signal Process.*, vol. 1, no. 1, pp. 147–155, Jun. 2007.
[10] C. Y. Chen and P. P. Vaidyanathan, "MIMO radar ambiguity properties and optimization using frequency-hopping waveforms," *IEEE Trans. Signal Process.*, vol. 56, no. 12, pp. 5926–5936, Dec. 2008.
[11] H. A. Khan and D. J. Edwards, "Doppler problems in orthogonal MIMO radars," in *Proc. IEEE Radar Conf.*, 2006, pp. 244–247.
[12] W. Q. Wang, "MIMO SAR OFDM chirp waveform diversity design with random matrix modulation," *IEEE Trans. Geosci. Remote Sens.*, vol. 53, no. 3, pp. 1615–1625, Mar. 2015.
[13] H. Deng, "Discrete frequency-coding waveform design for netted radar systems," *IEEE Signal Process. Lett.*, vol. 11, no. 2, pp. 179–182, Feb. 2004.
[14] H. Deng, "Polyphase code design for orthogonal netted radar systems," *IEEE Trans. Signal Process.*, vol. 52, no. 11, pp. 3126–3135, Nov. 2004.
[15] B. Liu, Z. He, and Q. He, "Optimization of orthogonal discrete frequency-coding waveform based on modified genetic algorithm for MIMO radar," in *Proc. Int. Conf. Commun., Circuits Syst.*, 2007, pp. 966–970.
[16] M. S. Willsey, K. M. Cuomo, and A. V. Oppenheim, "Quasi-orthogonal wideband radar waveforms based on chaotic systems," *IEEE Trans. Aerosp. Electron. Syst.*, vol. 47, no. 3, pp. 1974–1984, Jul. 2011.
[17] J. Yang, H. Q. Wang, W. D. Jiang, and Z. W. Zhuang, "Complementary-based chaotic phase-coded waveforms design for MIMO radar," *IET Radar Sonar Navig.*, vol. 7, no. 4, pp. 371–382, Apr. 2013.

[18] J. Yang, Z. K. Qiu, X. Li, and Z. W. Zhuang, "Uncertain chaotic behaviours of chaotic-based frequency- and phase-modulated signals," *IET Signal Process.*, vol. 5, no. 8, pp. 748–756, Dec. 2011.
[19] E. Okamoto and Y. Inaba, "A chaos MIMO transmission scheme using turbo principle for secure channel-coded transmission," *IEICE Trans. Commun.*, vol. E98, no. B8, pp. 1482–1491, Aug. 2015.
[20] F. Y. Lin and J. M. Liu, "Chaotic radar using nonlinear laser dynamics," *IEEE J. Quantum Electron.*, vol. 40, no. 6, pp. 815–820, Jun. 2004.
[21] S. Qiao *et al.*, "A new architecture of UWB radar utilizing microwave chaotic signals and chaos synchronization," *Progr. Electromagn. Res.*, vol. 75, pp. 225–237, 2007.
[22] T. Jiang *et al.*, "Simulation and experimental evaluation of the radar signal performance of chaotic signals generated from a microwave Colpitts oscillator," *Progr. Electromagn. Res.*, vol. 90, pp. 15–30, 2009.
[23] Y. Ji *et al.*, "Microwave-photonic sensor for remote water-level monitoring based on chaotic laser," *Int. J. Bifurcation Chaos*, vol. 24, no. 3, Mar. 2014, Art. ID 1450032.
[24] F. Y. Lin and J. M. Liu, "Ambiguity functions of laser-based chaotic radar," *IEEE J. Quantum Electron.*, vol. 40, no. 12, pp. 1732–1738, Dec. 2004.
[25] Z. G. Shi *et al.*, "Ambiguity functions of direct chaotic radar employing microwave chaotic Colpitts oscillator," *Progr. Electromagn. Res.*, vol. 77, pp. 1–14, 2007.
[26] F. Y. Lin and J. M. Liu, "Chaotic lidar," *IEEE J. Sel. Topics Signal Process.*, vol. 10, no. 5, pp. 991–997, Sep. 2004.
[27] W. T. Wu, Y. H. Liao, and F. Y. Lin, "Noise suppressions in synchronized chaos lidars," *Opt. Exp.*, vol. 18, no. 25, pp. 26155–26162, Nov. 2010.
[28] F. Y. Lin and J. M. Liu, "Diverse waveform generation using semiconductor lasers for radar and microwave applications," *IEEE J. Quantum Electron.*, vol. 40, no. 6, pp. 682–689, Jun. 2004.
[29] Y. H. Liao and F. Y. Lin, "Dynamical characteristics and their applications of semiconductor lasers subject to both optical injection and optical feedback," *Opt. Exp.*, vol. 21, no. 20, pp. 23568–23578, Sep. 2013.
[30] G. Mykolaitis, A. Tamasevicius, and S. Bumeliene, "Experimental demonstration of chaos from Colpitts oscillator in VHF and UHF ranges," *Electron. Lett.*, vol. 40, no. 2, pp. 91–92, Jan. 2004.
[31] A. Tamasevicius *et al.*, "Chaotic Colpitts oscillator for the ultrahigh frequency range," *Nonlinear Dyn.*, vol. 44, no. 1, pp. 159–165, Jun. 2006.
[32] J. Ohtsubo, *Semiconductor Lasers: Stability, Instability and Chaos*, 2nd ed. Berlin, Germany: Springer-Verlag, 2007.
[33] C. H. Cheng, Y. C. Chen, and F. Y. Lin, "Chaos time delay signature suppression and bandwidth enhancement by electrical heterodyning," *Opt. Exp.*, vol. 23, no. 3, pp. 2308–2319, Feb. 2015.
[34] X. Z. Li and S. C. Chan, "Heterodyne random bit generation using an optically injected semiconductor laser in chaos," *IEEE J. Quantum Electron.*, vol. 49, no. 10, pp. 829–838, Oct. 2013.
[35] J. Mork, B. Tromborg, and J. Mark, "Chaos in semiconductor lasers with optical feedback: Theory and experiment," *IEEE J. Quantum Electron.*, vol. 28, no. 1, pp. 93–108, Jan. 1992.
[36] R. Lang and K. Kobayashi, "External optical feedback effects on semiconductor injection laser properties," *IEEE J. Quantum Electron.*, vol. QE-16, no. 3, pp. 347–355, Mar. 1980.
[37] J. M. Liu and T. B. Simpson, "Four-wave mixing and optical modulation in a semiconductor laser," *IEEE J. Quantum Electron.*, vol. 30, no. 4, pp. 957–965, Apr. 1994.
[38] S. K. Hwang, J. M. Liu, and J. K. White, "35-GHz intrinsic bandwidth for direct modulation in 1.3-μm semiconductor lasers subject to strong injection locking," *IEEE Photon. Technol. Lett.*, vol. 16, no. 4, pp. 972–974, Apr. 2004.
[39] F. Y. Lin, Y. K. Chao, and T. C. Wu, "Effective bandwidths of broadband chaotic signals," *IEEE J. Quantum Electron.*, vol. 48, no. 8, pp. 1010–1014, Aug. 2012.